

# Theoretical analysis on quantum interference effect in fast-light media

Datang Xu<sup>1</sup>, Chaohua Tan<sup>1</sup>, and Guoxiang Huang<sup>1,2,a</sup>

<sup>1</sup>*State Key Laboratory of Precision Spectroscopy and Department of Physics,  
East China Normal University, Shanghai 200062, China*

<sup>2</sup>*NYU-ECNU Joint Physics Research Institute at NYU-Shanghai, Shanghai 200062, China*

(Dated: November 27, 2024)

## Abstract

We make a systematic theoretical analysis on the quantum interference (QI) effects in various fast-light media (including gain-assisted  $N$ , gain-assisted ladder-I, and gain-assisted ladder-II atomic systems). We show that such fast-light media are capable of not only completely eliminating the absorption but also suppressing the gain of signal field, and hence provide the possibility to realize a stable propagation of the signal field with a superluminal velocity. We find that there is a destructive (constructive) QI effect in gain-assisted ladder-I (gain-assisted  $N$ ) system, but no QI in the gain-assisted ladder-II system; furthermore, a crossover from destructive (constructive) QI to Autler-Townes splitting may occur for the gain-assisted ladder-I (gain-assisted  $N$ ) system when the control field of the system is modulated. Our theoretical analysis can be applied to other multi-level systems, and the results obtained may have promising applications in optical and quantum information processing and transmission.

PACS numbers: 42.50.Gy, 42.50.Ct

---

<sup>a</sup> gxhuang@phy.ecnu.edu.cn

## I. INTRODUCTION

In the past two decades, much attention has been paid to the study of slow light [1], which can be realized in various optical media [2]. The most typical system for obtaining slow light is the use of electromagnetically induced transparency (EIT) occurring in a three level  $\Lambda$ -type atomic system interacting with two resonant laser fields [3]. Slow light has many practical applications, including high-capacity communication networks, ultrafast all-optical information processing, precision spectroscopy and precision measurements, quantum computing and quantum information, and so on [1–3].

However, as pointed out in Ref. [4], EIT-based slow-light scheme has some drawbacks. Two of them are significant signal-field attenuation and spreading and very long response time. Parallel to the study of slow light, in recent years there are also tremendous interest on the investigation of fast light (also called superluminal light) [5–7]. Chu and Wong [8] firstly demonstrated a superluminal propagation of optical wave packet in an absorptive medium. In order to suppress the substantial attenuation of the optical wave packet occurred in the experiment [8], Chiao [9] proposed to use a gain medium with inverted atomic population to obtain a stable superluminal propagation. Steinberg and Chiao [10] proved that the stable superluminal propagation in the medium with a gain doublet is indeed possible. The works carried out by Wang *et al.* [11] and Biglow *et al.* [12], as well as those reported in Refs. [4, 13–22], further revealed many intriguing aspects of fast light, including the possibility of obtaining giant Kerr nonlinearity and superluminal optical solitons. Recently, it has been demonstrated that the use of fast-light media can realize quantum phase gates [23] and light and quantum memory [24, 25].

It is well known that the physical mechanism of EIT is the quantum interference (QI) effect contributed by control field, by which the absorption of signal field can be greatly suppressed, i.e. an EIT transparency window is opened in the absorption spectrum of the signal field. Furthermore, the QI also results in a drastic change of dispersion and hence a large reduction of the group velocity of the signal field [1–3]. In addition, it has been discovered recently that in such systems there exists an interesting crossover from EIT to Autler-Townes splitting (ATS) [26–36]. It is natural to ask the question: Is it possible to have similar phenomena for fast-light media?

In this article, we give a definite answer to this question by investigating the absorption

spectra of several typical fast-light media, including gain-assisted  $N$  (GAN), gain-assisted ladder-I (GAL-I), and gain-assisted ladder-II (GAL-II) atomic systems (Fig. 1). We carry out systematic theoretical analyses and give clear physical explanations on the QI effects occurring in these fast-light media by extending the spectrum-decomposition method (SDM) developed recently for the EIT-ATS crossover of slow light [26–36]. We show that such fast-light media are capable of not only completely eliminating the absorption but also suppressing the gain of signalmodulate field, and hence provide the possibility to realize a stable long-distance propagation of the signal field with a superluminal velocity. We find that there is a destructive (constructive) QI effect in the GAL-I (GAN) system, but no QI in the GAL-II system; furthermore, a crossover from destructive (constructive) QI to ATS may occur for the GAL-I (GAN) system if the control field of the system is modulated. Our theoretical analysis can be applied to other gain-assisted multi-level systems (e.g. quantum dots, rare-earth ions in crystals, etc.), and the results obtained may have promising applications in optical and quantum information processing and transmission.

The remainder of the article is organized as follows. In Sec. II, we present the model and analyze the QI effect in the GAN system. In Sec. III and Sec. IV, we carry out similar analyses and provide related results for the GAL-I and GAL-II systems, respectively. Finally, in Sec. V we give a discussion and a summary of the main results obtained in this work.

## II. QUANTUM INTERFERENCE CHARACTERS OF THE GAN SYSTEM

### A. Model and linear dispersion relation

We first consider a cold atomic system with the GAN-type level configuration (Fig. 1(a)). The quantum states  $|1\rangle$  and  $|3\rangle$  are coupled by a strong, continuous-wave (CW) pump field (with half Rabi frequency  $\Omega_p$ ),  $|2\rangle$  and  $|3\rangle$  are coupled by a weak, pulsed signal field (with half Rabi frequency  $\Omega_s$ ), and  $|2\rangle$  and  $|4\rangle$  are coupled by a strong, CW control field (with half Rabi frequency  $\Omega_c$ ), respectively.  $\Delta_j$  ( $j = 2, 3, 4$ ) are detunings, and dashed arrows denote the spontaneous-emission rates ( $\Gamma_{13}, \Gamma_{14}, \Gamma_{24}$ ). Such system, where the states  $|j\rangle$  ( $j = 1, 2, 3$ ), the pump field ( $\Omega_p$ ) and signal field ( $\Omega_s$ ) constitutes a core of active Raman gain (ARG) [14–16], has attracted considerable attention recently [4, 13, 17, 18, 22].

We assume the pump, signal, and control fields propagate in  $z$  direction, the electric field

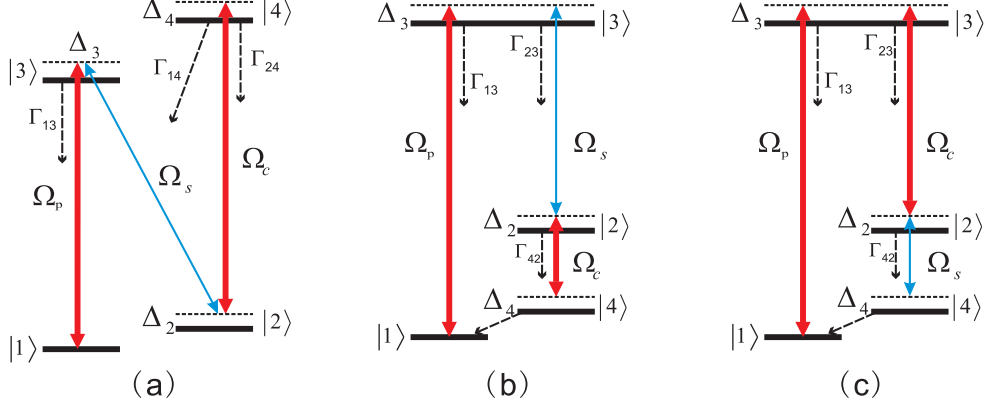


FIG. 1. (Color online) Excitation schemes of four-state atoms with the level configuration of the form (a) GAN system, (b) GAL-I system, and (c) GAL-II system. In each system, four quantum states  $|1\rangle$ ,  $|2\rangle$ ,  $|3\rangle$ , and  $|4\rangle$  are coupled by a pump field  $\mathbf{E}_p$  (with half Rabi frequency  $\Omega_p$ ), a signal field  $\mathbf{E}_s$  (with half Rabi frequency  $\Omega_s$ ), and a control field  $\mathbf{E}_c$  (with half Rabi frequency  $\Omega_c$ ) in different ways.  $\Delta_j$  ( $j = 2, 3, 4$ ) are detunings. The dashed arrows represent the spontaneous emission or incoherent population exchange rates (i.e.  $\Gamma_{13}$ ,  $\Gamma_{14}$ ,  $\Gamma_{24}$ ,  $\Gamma_{23}$ ,  $\Gamma_{42}$ ).

vector acting in the system reads  $\mathbf{E} = \mathbf{E}_p + \mathbf{E}_s + \mathbf{E}_c = \sum_{l=p,s,c} \mathbf{e}_l \mathcal{E}_l \exp[i(k_l z - \omega_l t)] + \text{c.c.}$ , where  $\mathbf{e}_l$  ( $k_l$ ) is the unit polarization vector (wavenumber) of the electric-field component with the envelope  $\mathcal{E}_l$  ( $l = p, s, c$ ). Under electric-dipole and rotating-wave approximations, the interaction Hamiltonian of the system interacting with laser fields reads  $\hat{\mathcal{H}}_{\text{int}} = -\hbar \left[ \sum_{j=1}^4 \Delta_j |j\rangle \langle j| + (\Omega_p |3\rangle \langle 1| + \Omega_s |3\rangle \langle 2| + \Omega_c |4\rangle \langle 2| + \text{h.c.}) \right]$ , where h.c. represents Hermitian conjugation,  $\Omega_p = (\mathbf{p}_{31} \cdot \mathcal{E}_p) / \hbar$ ,  $\Omega_s = (\mathbf{p}_{32} \cdot \mathcal{E}_s) / \hbar$ , and  $\Omega_c = (\mathbf{p}_{42} \cdot \mathcal{E}_c) / \hbar$  are respectively the half Rabi frequencies of the pump, signal, and control fields, with  $\mathbf{p}_{jl}$  being the electric-dipole matrix element associated with the transition from state  $|j\rangle$  to state  $|l\rangle$ .

Under electric-dipole approximation (EDA) and rotating-wave approximation (RWA), the dynamics of the system is governed by the Bloch equation [37]

$$i\hbar \left( \frac{\partial}{\partial t} + \hat{\Gamma} \right) \sigma = \left[ \hat{\mathcal{H}}_{\text{int}}, \sigma \right], \quad (1)$$

where  $\sigma$  is a  $4 \times 4$  density matrix in the interaction picture, and  $\hat{\Gamma}$  is a  $4 \times 4$  relaxation matrix describing the spontaneous emission and dephasing. The explicit expression of Eq. (1) is presented in Appendix A.

As in Ref. [4], we assume the one-photon detuning  $\Delta_3$  is much larger than all the Rabi frequencies, Doppler broadened line width (resulted by the thermal motion of the atoms),

atomic coherence decay rates, and frequency shift induced by the pump and control fields. In this situation, the population keeps mainly in the ground state  $|1\rangle$  to guarantee the system working in fast-light regime; furthermore, Doppler effect can be largely suppressed. However, the (remanent) Doppler effect still has influence on the QI property of the GAN and GAL-II systems (but not in the GAL-I system), as shown in Sec. V.

From the Maxwell equation  $\nabla^2 \mathbf{E}_s - (1/c^2)\partial^2 \mathbf{E}_s/\partial t^2 = (1/\epsilon_0 c^2)\partial^2 \mathbf{P}_s/\partial t^2$  with the electric polarization intensity  $\mathbf{P}_s = \mathcal{N}_a(\mathbf{p}_{23}\sigma_{32} e^{i(k_s z - \omega_s t)} + \text{c.c.})$ , one can obtain the equation of motion for the Rabi frequency of the signal field under slowly-varying envelope approximation (SVEA), which reads

$$i \left( \frac{\partial}{\partial z} + \frac{1}{c} \frac{\partial}{\partial t} \right) \Omega_s + \kappa_{23}\sigma_{32} = 0, \quad (2)$$

where  $\kappa_{23} = \mathcal{N}_a \omega_s |\mathbf{p}_{32}|^2 / (2\hbar \epsilon_0 c)$  with  $\mathcal{N}_a$  the atomic density. Note that in deriving the above equation we have assumed the signal-field envelope is wide enough in the transverse (i.e.  $x$ ,  $y$ ) directions, so that the diffraction term  $(\partial^2/\partial x^2 + \partial^2/\partial y^2)\Omega_s$  can be disregarded.

The base state of the system (i.e. the steady-state solution of the Maxwell-Bloch (MB) Eqs. (1) and (2) for  $\Omega_s = 0$ ) is  $\sigma_{11}^{(0)} = \Gamma_{14}|\Omega_c|^2(\Gamma_3 X_{31} + |\Omega_p|^2)/D$ ,  $\sigma_{22}^{(0)} = \Gamma_{23}|\Omega_p|^2(\Gamma_4 X_{42} + |\Omega_c|^2)/D$ ,  $\sigma_{33}^{(0)} = \Gamma_{14}|\Omega_c|^2|\Omega_p|^2/D$ ,  $\sigma_{44}^{(0)} = \Gamma_{23}|\Omega_c|^2|\Omega_p|^2/D$ ,  $\sigma_{31}^{(0)} = -\Omega_p \Gamma_{14} \Gamma_3 X_{31} |\Omega_c|^2 / (d_{31} D)$ ,  $\sigma_{42}^{(0)} = -\Omega_c \Gamma_{23} \Gamma_4 X_{42} |\Omega_p|^2 / (d_{42} D)$ , with  $X_{31} = |d_{31}|^2 / (2\gamma_{31})$ ,  $X_{42} = |d_{42}|^2 / (2\gamma_{42})$  and  $D = \Gamma_{14}|\Omega_c|^2(\Gamma_3 X_{31} + 2|\Omega_p|^2) + \Gamma_{23}|\Omega_p|^2(\Gamma_4 X_{42} + 2|\Omega_c|^2)$ . Here the meaning of the quantities  $\Gamma_{jl}$  and  $d_{jl}$  has been explained in the Appendix A. For large  $\Delta_3$  one has  $\sigma_{11}^{(0)} \approx 1$ ,  $\sigma_{31}^{(0)} \approx -\Omega_p/d_{31}$ , and all other  $\sigma_{jl}^{(0)} \approx 0$ , which means that initially the atomic medium is prepared with the population mainly in the ground state state  $|1\rangle$ .

The base state of this system will evolve into a time-dependent state when the weak signal field is switched on [38]. Solving the MB Eqs. (1) and (2) we obtain the solution

$$\Omega_s = F e^{i\theta}, \quad (3a)$$

$$\sigma_{32}^{(1)} = \frac{B(\sigma_{33}^{(0)} - \sigma_{22}^{(0)}) - (D_p + |\Omega_c|^2)\Omega_p \sigma_{31}^{*(0)} - (D_c + |\Omega_p|^2)\Omega_c \sigma_{42}^{*(0)}}{(\omega + d_{32})B - |\Omega_p|^2(D_p + |\Omega_c|^2) - |\Omega_c|^2(D_c + |\Omega_p|^2)} F e^{i\theta}, \quad (3b)$$

where  $F$  is an envelope (its concrete form is not needed here),  $\theta = K(\omega)z - \omega t$  [39],  $D_p = (\omega - d_{41}^*)(\omega - d_{43}^*) - |\Omega_p|^2$ ,  $D_c = (\omega - d_{21}^*)(\omega - d_{41}^*) - |\Omega_c|^2$ , and  $B = (\omega - d_{21}^*)(\omega - d_{41}^*)(\omega - d_{43}^*) - (\omega - d_{21}^*)|\Omega_p|^2 - (\omega - d_{43}^*)|\Omega_c|^2$ . Explicit expressions of the other first-order solutions for  $\sigma_{jl}^{(1)}$  ( $j \neq 3, l \neq 2$ ) are omitted here.

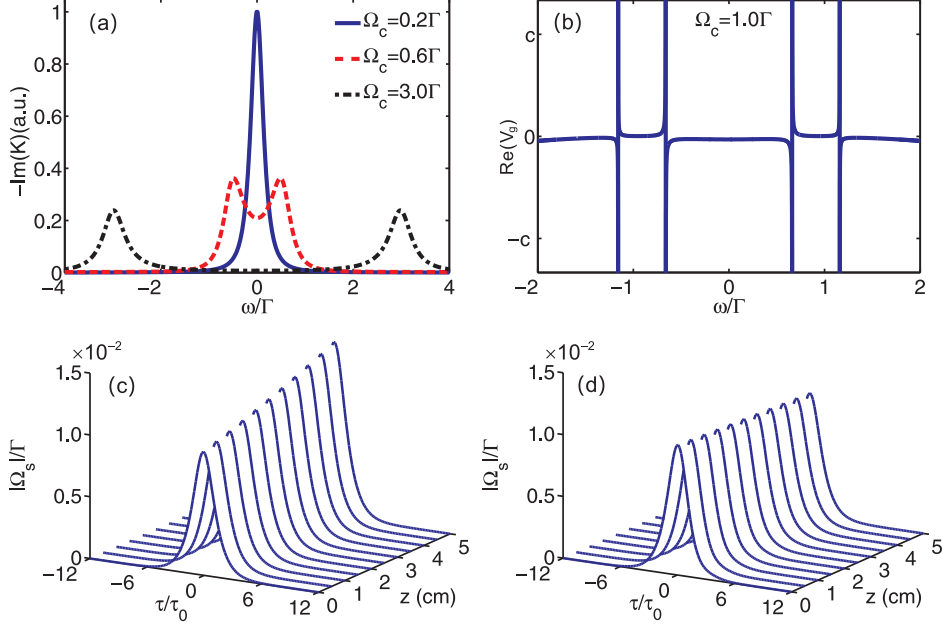


FIG. 2. (Color online) (a) Gain spectrum of the signal field,  $-\text{Im}(K)$ , as a function of  $\omega/\Gamma$  and  $\Omega_c$  for the GAN system. When  $\Omega_c = 0.2\Gamma$  it has only a single peak (blue solid line). For  $\Omega_c = 0.6\Gamma$  a gain doublet appears (red dashed line) and the doublet becomes wide by increasing  $\Omega_c$  ( $= 3.0\Gamma$ ) (black dotted-dashed line). (b) Group velocity of the signal field,  $\text{Re}(V_g)$ , as a function of  $\omega/\Gamma$  for  $\Omega_c = 1.0\Gamma$ , which can be smaller than  $c$  (subluminal), larger than  $c$  and even negative (superluminal). (c) ((d)) Numerical result for  $|\Omega_s|/\Gamma$  as function of  $\tau/\tau_0$  ( $\tau_0 = 1.0 \times 10^{-6}$  s) and  $z$  for  $\Omega_c = 0.2\Gamma$  ( $\Omega_c = 3.0\Gamma$ ).

The linear dispersion relation of the system reads

$$K(\omega) = \frac{\omega}{c} + \kappa_{23} \frac{B(\sigma_{33}^{(0)} - \sigma_{22}^{(0)}) - (D_p + |\Omega_c|^2)\Omega_p\sigma_{31}^{*(0)} - (D_c + |\Omega_p|^2)\Omega_c\sigma_{42}^{*(0)}}{(\omega + d_{32})B - |\Omega_p|^2(D_p + |\Omega_c|^2) - |\Omega_c|^2(D_c + |\Omega_p|^2)}. \quad (4)$$

The group velocity of the signal field is given by  $V_g = [\partial \text{Re}(K)/\partial \omega]^{-1}$ .

Shown in Fig. 2(a) is the gain spectrum of the signal field, i.e.  $-\text{Im}(K)$ , as a function of  $\omega/\Gamma$  and  $\Omega_c$ . When plotting the figure, we have chosen the atomic vapor of  $^{85}\text{Rb}$  with the states assigned by  $|1\rangle = |5^2S_{1/2}, F = 2, m_F = -1\rangle$ ,  $|2\rangle = |5^2S_{1/2}, F = 3, m_F = 1\rangle$ ,  $|3\rangle = |5^2P_{1/2}, F = 2, m_F = 0\rangle$ , and  $|4\rangle = |5^2P_{3/2}, F = 4, m_F = 2\rangle$ . The system parameters are given by  $\Gamma = 6$  MHz,  $\Gamma_3 = \Gamma_4 = \Gamma$ ,  $\Gamma_{13} = \Gamma_{23} = \Gamma_{14} = \Gamma_{24} = \Gamma/2$ ,  $\gamma_{21} = 10$  kHz,  $\Delta_2 = \Delta_4 = 0$ ,  $\Delta_3 = 0.5$  GHz,  $\Omega_p = 1.0\Gamma$ , and  $\kappa_{23}/\Gamma = 10^3 \text{ cm}^{-1}$ . From the figure we see that when the control field is weak ( $\Omega_c = 0.2\Gamma$ ) the gain spectrum has only a single peak near  $\omega = 0$  (blue solid line). Interestingly, the single peak will become two peaks if

the condition

$$|\Omega_c|^2 > \frac{\kappa_{23}|\Omega_p|^2\gamma_{41}}{\Delta_3^2} \quad (5)$$

is satisfied. Illustrated by the red dashed line in Fig. 2(a) is for  $\Omega_c = 0.6\Gamma$ . In this case the condition (5) is fulfilled and hence a gain doublet (a dip between two gain peaks) appears in the gain spectrum. By increasing  $\Omega_c$  to  $3.0\Gamma$ , the distance between the two peaks becomes wide and the gain of the signal field is nearly vanishing at  $\omega = 0$  (black dotted-dashed line). The appearance of the gain doublet in the gain spectrum is due to a QI effect in the system, which will be explained in the next subsection.

Fig. 2(b) shows the group velocity  $\text{Re}(V_g)$  of the signal pulse as a function of  $\omega/\Gamma$  when control field  $\Omega_c = 1.0\Gamma$ . The system parameters used are the same as in Fig. 2(a). We see that  $\text{Re}(V_g)$  can be smaller than  $c$  (subluminal), larger than  $c$  and even negative (superluminal). Especially, at  $\omega = 0$  we have  $\text{Re}(V_g) = -0.51 \times 10^{-3}c$ . Hence the atomic system with GAN level configuration is indeed a fast-light medium.

In addition to acquire QI and hence the gain doublet in the gain spectrum, the introduction of the control field can also stabilize the propagation of the signal pulse. Shown in Fig. 2(c) is the numerical result based on the MB Eqs. (1) and (2) for  $|\Omega_s|/\Gamma$  as function of  $\tau/\tau_0$  and  $z$  for  $\Omega_c = 0.2\Gamma$ , where  $\tau = t - z/\text{Re}(V_g)$  is traveling coordinate and  $\tau_0 = 1.0 \times 10^{-6}$  s is initial pulse width. In this case (weak control field), the signal pulse has a large gain and hence a significant deformation happens during propagation. However, for a large control field ( $\Omega_c = 3.0\Gamma$ ), the gain is largely suppressed and hence no deformation occurs during the propagation of the signal pulse. In the numerical simulation, we have taken the initial signal pulse with the form  $\Omega_s = 0.01\Gamma, \text{sech}(\tau/\tau_0)$ . From these results we conclude that the GAN system with a large control field can support a stable propagation of the signal field.

## B. Crossover from constructive QI to ATS in the GAN system

Now we make a detailed analysis on the appearance of gain doublet in the gain spectrum of the signal field shown above by using the SDM developed recently for slow-light media [26–36].

To this end, we simplify the linear dispersion relation (i.e. Eq. (4)). Under the condition  $\Delta_3 \gg \gamma_{ij}, \Gamma_{ij}, \Omega_p, \Omega_c$ , Eq. (4) for  $\Delta_2 = \Delta_4 = 0$  can be reduces to the form  $K(\omega) = \omega/c + \tilde{\kappa}_{23}(\omega + i\gamma_{41})/[(\omega + i\gamma_{21})(\omega + i\gamma_{41}) - |\Omega_c|^2]$ , with  $\tilde{\kappa}_{23} = \kappa_{23}\Omega_p\sigma_{31}^{(0)*}/\Delta_3$ . One can also obtain a

similar expression of  $K(\omega)$  for nonvanishing  $\Delta_2$  and  $\Delta_4$ , but it is lengthy and thus omitted here.  $K(\omega)$  can be written into the form

$$K(\omega) = \frac{\omega}{c} + \tilde{\kappa}_{23} \frac{\omega + i\gamma_{41}}{(\omega - \omega_+)(\omega - \omega_-)}, \quad (6)$$

where  $\omega_{\pm} = -i(\gamma_{21} + \gamma_{41})/2 \pm [(|\Omega_c|^2 - |\Omega_{\text{ref}}|^2)]^{1/2}$ , with  $\Omega_{\text{ref}} = |\gamma_{21} - \gamma_{41}|/2$  (reference half Rabi frequency).

In order to illustrate the QI effect in a simple and clear way, as done in Refs. [26–36], we decompose the gain spectrum  $-\text{Im}(K)$  for different regions of  $\Omega_c$  as follows.

(i). *Weak control field region* ( $|\Omega_c| < \Omega_{\text{ref}} \approx \gamma_{14}/2$ ): Equation (6) can be decomposed as

$$K(\omega) = \frac{\omega}{c} + \tilde{\kappa}_{23} \left( \frac{A_+}{\omega - \omega_+} + \frac{A_-}{\omega - \omega_-} \right), \quad (7)$$

with  $A_{\pm} = \pm(\omega_{\pm} + i\gamma_{41})/(\omega_+ - \omega_-)$ . Since in this region  $\text{Re}(\omega_{\pm}) = \text{Im}(A_{\pm}) = 0$ , we obtain the gain spectrum

$$-\text{Im}(K) = -\tilde{\kappa}_{23} \left( \frac{B_+}{\omega^2 + \delta_+^2} + \frac{B_-}{\omega^2 + \delta_-^2} \right) = -L_+ - L_-, \quad (8)$$

where  $\delta_{\pm} = \text{Im}(\omega_{\pm})$ ,  $B_{\pm} = A_{\pm}\delta_{\pm}$ , and  $L_{\pm} = \tilde{\kappa}_{23}B_{\pm}/(\omega^2 + \delta_{\pm}^2)$ . Thus the signal field gain spectrum comprises two Lorentzians centered at  $\omega = 0$ .

Shown in Fig. 3(a) is the result of  $-L_+$ , which has a large positive single peak (red dashed line), and  $-L_-$ , which has a negative (concave but very shallow) single peak (black dashed-dotted line). When plotting the figure, a small control field ( $\Omega_c = 0.2\Gamma$ ) is taken. We see that although for small  $\Omega_c$  there is a destructive interference between  $-L_+$  and  $-L_-$ , the interference is too small and hence can be neglected. So the superposition of  $-L_+$  and  $-L_-$  is contributed mainly by  $-L_+$ . As a result, the gain spectrum  $-\text{Im}(K)$  displays only a single peak (blue solid line).

(ii). *Intermediate control field region* ( $|\Omega_c| > \Omega_{\text{ref}}$ ): In this region  $\text{Re}(\omega_{\pm}) \neq 0$ , we obtain

$$-\text{Im}(K) = \frac{\tilde{\kappa}_{23}}{2} \left\{ \frac{W}{(\omega - \delta)^2 + W^2} + \frac{W}{(\omega + \delta)^2 + W^2} + \frac{g}{\delta} \left[ \frac{\omega - \delta}{(\omega - \delta)^2 + W^2} - \frac{\omega + \delta}{(\omega + \delta)^2 + W^2} \right] \right\}, \quad (9)$$

with  $W = (\gamma_{21} + \gamma_{41})/2$ ,  $\delta = \sqrt{4|\Omega_c|^2 - (\gamma_{21} - \gamma_{41})^2}/2$ , and  $g = (\gamma_{21} - \gamma_{41})/2$ . The previous two terms in the bracket  $\{\dots\}$  of the above expression (i.e. the two Lorentzian terms) can be thought as the net contribution contributed to the gain resonance from two different



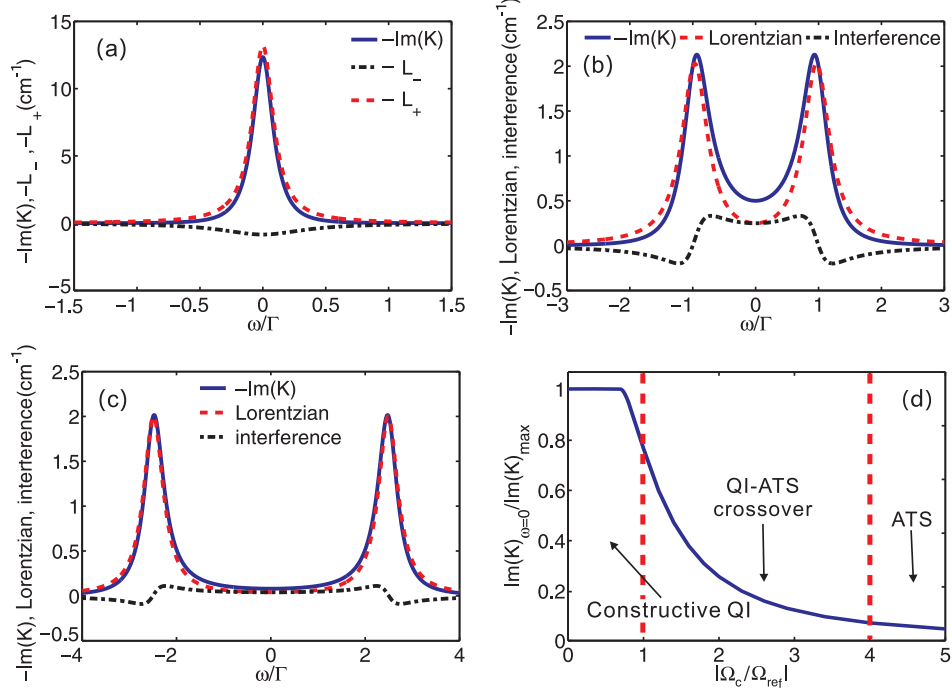


FIG. 3. (Color online) (a)  $-\text{Im}(K)$  in the weak control field region ( $\Omega_c = 0.2\Gamma < \Omega_{\text{ref}}$ ) as a function of  $\omega/\Gamma$ . The red dashed (the black dashed-dotted) line is for  $-L_+$  ( $-L_-$ ); the blue solid line is for  $-\text{Im}(K)$ . (b) Gain spectrum in the intermediate control field region ( $\Omega_c = 1.0\Gamma < \Omega_{\text{ref}}$ ). Red dashed line is for two Lorentzian terms; black dashed-dotted line is for constructive QI term; blue solid line is for  $-\text{Im}(K)$ . (c) Gain spectrum in the strong control field region ( $\Omega_c = 2.5\Gamma > \Omega_{\text{ref}}$ ). Red dashed line is for two Lorentzian terms; black dashed-dotted line is for small constructive QI term; blue solid line is for  $-\text{Im}(K)$ . (d) The “phase diagram” of  $\text{Im}(K)_{\omega=0}/\text{Im}(K)_{\text{max}}$  as a function of  $|\Omega_c/\Omega_{\text{ref}}|$  illustrating the transition from constructive QI to ATS in the GAN system. Three regions (i.e. constructive QI region, the QI-ATS crossover region, and the ATS region) are separated by two vertical dashed lines.

channels corresponding to the two dressed states (i.e. the states  $|2\rangle$  and  $|4\rangle$ ) created by the control field  $\Omega_c$ . The term proportional to  $g$  is clearly a QI term. The QI is controlled by the parameter  $g$  and it is destructive (constructive) if  $g > 0$  ( $g < 0$ ). Since in the GAN system  $\gamma_{21}$  is always much smaller than  $\gamma_{41}$  and  $g$  is often negative, thus the QI in the system is a constructive one.

Fig. 3(b) shows the gain spectrum in the intermediate control field region ( $|\Omega_c| = 1.0\Gamma > \Omega_{\text{ref}}$ ). The red dashed line is for the two Lorentzian terms; the black dashed-dotted line is

for the constructive QI term; the blue solid line is for  $-\text{Im}(K)$ . We see that in this region a gain doublet appears, which is the result of the superposition of the two Lorentzian terms and the QI term.

(iii). *Large control field region* ( $|\Omega_c| \gg \Omega_{\text{ref}}$ ): In this case, the gain spectrum is still given by (9), but the strength of the QI term,  $g/\delta$ , is very weak (i.e.  $g/\delta \approx 0$ ). Thus one has

$$-\text{Im}(K) \approx \frac{\tilde{\kappa}_{23}}{2} \left[ \frac{W}{(\omega - \delta)^2 + W^2} + \frac{W}{(\omega + \delta)^2 + W^2} \right]. \quad (10)$$

Shown in Fig. 3(c) is the gain spectrum as a function of  $\omega/\Gamma$  for  $|\Omega_c| = 2.5\Gamma \gg \Omega_{\text{ref}}$ . The red dashed line represents the contribution by the sum of the two Lorentzian terms. For illustration, we have also plotted the contribution from the small QI term (omitted in Eq. (10)), denoted by the black dotted-dashed line. We see that in this case the QI is small and weak constructive. The blue solid line is the curve of  $-\text{Im}(K)$ , which has two resonance peaks at  $\omega \approx \pm\Omega_c$ . Obviously, the phenomenon found in this case belongs to ATS because the window of the gain doublet is mainly due to the contribution by the two Lorentzian terms. From the results given in Fig. 3(b) and Fig. 3(c), we conclude that the GAN system possesses indeed QI effect and allows a crossover from the QI to the ATS.

Fig. 3(d) shows the “phase diagram” that illustrates the crossover from the constructive QI effect to the ATS in the GAN system by plotting  $\text{Im}(K)_{\omega=0}/\text{Im}(K)_{\text{max}}$  as a function of  $|\Omega_c/\Omega_{\text{ref}}|$ . We see that the phase diagram can be roughly divided into three regions, i.e. the constructive QI region (weak control field region), the QI-ATS crossover region (intermediate control field region), and the ATS region (large control field region), very similar to that found in various EIT systems reported recently for slow lights [26–36].

The physical reason for the occurrence of the QI (i.e. the gain doublet in the gain spectrum in Fig. 3(a)) can be explained as follows. From the Hamiltonian give above we obtain an eigenstate of the system

$$|\psi\rangle = \left[ 1 + \frac{|\Omega_s|^2 d_4}{(|\Omega_c|^2 - d_2 d_4) d_3} \right] |1\rangle - \frac{\Omega_p \Omega_s^* d_4}{(|\Omega_c|^2 - d_2 d_4) d_3} |2\rangle - \frac{\Omega_p}{d_3} |3\rangle + \frac{\Omega_p \Omega_c \Omega_s^*}{(|\Omega_c|^2 - d_2 d_4) d_3} |4\rangle, \quad (11)$$

with  $d_2 = \Delta_2 + i\Gamma_2$ ,  $d_3 = \Delta_3 + i\Gamma_3$ ,  $d_4 = \Delta_4 + i\Gamma_4$ . For large  $\Delta_3$  and  $\Omega_c$  and for small  $\Delta_2$  and  $\Delta_4$ , the eigenstate (11) becomes  $|\psi\rangle \approx |1\rangle - (\Omega_p/\Delta_3)|3\rangle + [\Omega_p \Omega_c \Omega_s^*/(|\Omega_c|^2 \Delta_3)] |4\rangle$ , i.e. the atomic state  $|2\rangle$  is not involved. Such state is a “dark state” with zero eigenvalue resulted from the quantum interference between the transition paths  $|3\rangle \rightarrow |2\rangle$  and  $|4\rangle \rightarrow |2\rangle$ . As a result, the gain is largely suppressed and hence the gain doublet appears in the gain spectrum of the signal field.

### III. QUANTUM INTERFERENCE CHARACTERS OF THE GAL-I SYSTEM

#### A. Model and linear dispersion relation

We now turn to consider the GAL-I system shown in Fig. 1(b). The differences between the GAL-I system and the GAN system (Fig. 1(a)) are that in the GAL-I system the state  $|4\rangle$  is below the state  $|2\rangle$ . It is just these two differences that makes the QI character of the GAL-I system very different from that in the GAN system, as shown below.

Under EDA and RWA, in interaction picture the Hamiltonian of the GAL-I system is given by  $\hat{\mathcal{H}} = -\hbar[\sum_{j=1}^4 \Delta_j |j\rangle\langle j| + (\Omega_p |3\rangle\langle 1| + \Omega_s |3\rangle\langle 2| + \Omega_c |2\rangle\langle 4| + \text{h.c.})]$ , where the definitions of  $\Omega_p$  and  $\Omega_s$  are the same as those in the GAN system, but now  $\Omega_c = (\mathbf{p}_{24} \cdot \mathcal{E}_c)/\hbar$ . The Bloch equation of the system is presented in Appendix B. The equation of motion for  $\Omega_s$  can be derived by the Maxwell equation under SVEA, which reads

$$i \left( \frac{\partial}{\partial z} + \frac{1}{c} \frac{\partial}{\partial t} \right) \Omega_s + \kappa_{23} \sigma_{32} = 0, \quad (12)$$

with  $\kappa_{23} = \mathcal{N}_a \omega_s |\mathbf{p}_{32}|^2 / (2\hbar \varepsilon_0 c)$ .

The base state solution of the system can be obtained by using the MB equations Eqs. (B1), Eqs. (B2) and Eq. (12). For large  $\Delta_3$ , it reads  $\sigma_{11}^{(0)} \approx 1$ ,  $\sigma_{31}^{(0)} \approx -\Omega_p/d_{31}$ , and all other  $\sigma_{jl}^{(0)} \approx 0$  (see Appendix B), i.e. the atomic medium is initially prepared with the population mainly in the ground state state  $|1\rangle$ . When the weak signal field is applied, the solution at the first order of  $\Omega_s$  reads

$$\Omega_s = F e^{i\theta}, \quad (13a)$$

$$\sigma_{32}^{(1)} = \frac{B(\sigma_{33}^{(0)} - \sigma_{22}^{(0)}) - (D_p + |\Omega_c|^2)\Omega_p \sigma_{31}^{*(0)} - (D_c + |\Omega_p|^2)\Omega_c \sigma_{42}^{*(0)}}{(\omega + d_{32})B - |\Omega_p|^2(D_p + |\Omega_c|^2) - |\Omega_c|^2(D_c + |\Omega_p|^2)} F e^{i\theta}, \quad (13b)$$

where  $D_p = (\omega - d_{41}^*)(\omega - d_{43}^*) - |\Omega_p|^2$ ,  $D_c = (\omega - d_{21}^*)(\omega - d_{41}^*) - |\Omega_c|^2$  and  $B = (\omega - d_{21}^*)(\omega - d_{41}^*)(\omega - d_{43}^*) - (\omega - d_{21}^*)|\Omega_p|^2 - (\omega - d_{43}^*)|\Omega_c|^2$ . The linear dispersion relation of the system reads

$$K = \frac{\omega}{c} + \kappa_{23} \frac{B(\sigma_{33}^{(0)} - \sigma_{22}^{(0)}) - (D_p + |\Omega_c|^2)\Omega_p \sigma_{31}^{*(0)} - (D_c + |\Omega_p|^2)\Omega_c \sigma_{42}^{*(0)}}{(\omega + d_{32})B - |\Omega_p|^2(D_p + |\Omega_c|^2) - |\Omega_c|^2(D_c + |\Omega_p|^2)}. \quad (14)$$

In Fig. 4(a) we show the gain spectrum of the GAL-I system, i.e.  $-\text{Im}(K)$ , as a function of  $\omega/\Gamma$  and  $\Omega_c$ . States  $|1\rangle$  and  $|3\rangle$  in the system are assumed to be coupled with a pump field through a two-photon transition (with effective half Rabi frequency  $\Omega_p$ ). When plotting the

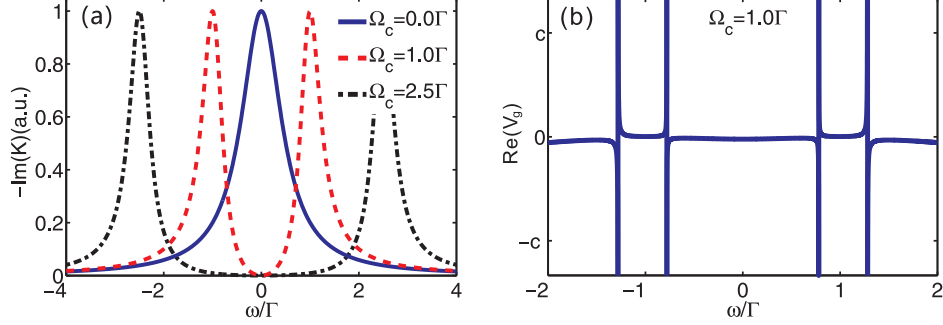


FIG. 4. (Color online) (a) Gain spectrum of the signal field,  $-\text{Im}(K)$ , as a function of  $\omega/\Gamma$  and  $\Omega_c$  for the GAL-I system. For  $\Omega_c = 0$ , it has only a single peak (blue solid line). For  $\Omega_c = 1.0\Gamma$ , a gain doublet appears (red dashed line) and the doublet becomes wide when  $\Omega_c = 2.5\Gamma$  (black dotted-dashed line). (b) Group velocity of the signal field,  $\text{Re}(V_g)$ , as a function of  $\omega/\Gamma$  for  $\Omega_c = 1.0\Gamma$ , which can be smaller than  $c$  (subluminal), larger than  $c$  and even negative (superluminal).

figure we also use the atomic vapor of  $^{85}\text{Rb}$ , with the levels assigned as  $|1\rangle = |5^2S_{1/2}, F = 2, m_F = -1\rangle$ ,  $|2\rangle = |5^2P_{1/2}, F = 2, m_F = 0\rangle$ ,  $|3\rangle = |5^2D_{5/2}, F = 3, m_F = -1\rangle$ , and  $|4\rangle = |5^2S_{1/2}, F = 3, m_F = 1\rangle$ . The system parameters used are  $\Gamma = 6$  MHz,  $\Gamma_3 = \Gamma$ ,  $\Gamma_{13} = \Gamma_{23} = \Gamma_{42} = 0.5\Gamma$ ,  $\gamma_{41} = 10$  kHz,  $\Delta_2 = \Delta_4 = 0$ ,  $\Delta_3 = 0.5$  GHz,  $\Omega_p = 0.5\Gamma$ , and  $\kappa_{23}/\Gamma = 10^3$  cm $^{-1}$ . One sees that for  $\Omega_c = 0$  the gain spectrum has only a single peak (blue solid line). Increasing  $\Omega_c$  to satisfy the condition  $|\Omega_c|^2 > \kappa_{23}|\Omega_p|^2\gamma_{41}/\Delta_3^2$  (the same as the condition (5)), a gain doublet appears. The red dashed line in the figure is the result for  $\Omega_c = 1.0\Gamma$ . When  $\Omega_c = 2.5\Gamma$ , the gain doublet becomes wide. The occurrence of the gain doublet is due to a QI effect in the system.

By inspection of Fig. 2(a) and Fig. 4(a), we find that there are some similar physical characters between them. First, when  $\Omega_c$  is small, Gain spectrum has only a single peak. Second, increasing  $\Omega_c$  to a critical value (i.e.  $\Omega_c > [\kappa_{23}|\Omega_p|^2\gamma_{41}/\Delta_3^2]^{1/2}$ ) the single peak becomes two peaks. By increasing  $\Omega_c$  further, the width between the two peaks increases. However, there are some differences between Fig. 2(a) and Fig. 4(a). The most obvious one is that the peak values of  $-\text{Im}(K)$  in Fig. 2(a) are reduced rapidly when  $\Omega_c$  is increased, but such phenomenon does not occur in Fig. 4(a). One of physical reasons is that in the GAN system (Fig. 2(a)) the level  $|4\rangle$  is above the level  $|2\rangle$  and the large  $\Gamma_{24}$  (the spontaneous emission rate from  $|4\rangle$  to  $|2\rangle$ ) contributes a population to  $|2\rangle$  and hence reduces the gain of the signal field significantly. Differently, in the GAL-I system (Fig. 4(a)) the level  $|4\rangle$

is below the level  $|2\rangle$  and  $\Gamma_{42}$  (the spontaneous emission rate from  $|2\rangle$  to  $|4\rangle$ ) is small and hence it has no significant influence to the gain spectrum. As a result, the peak values in the gain spectrum of the GAL-I system has no significant change as  $\Omega_c$  is increased.

Fig. 4(b) shows the group velocity of the signal pulse as a function of  $\omega/\Gamma$  for  $\Omega_c = 1.0\Gamma$ . The system parameters used for plotting the figure are the same as those in Fig. 4(a). One sees that  $\text{Re}(V_g)$  can be smaller and larger than  $c$ , and even negative, and hence the GAL-I system is a typical fast-light medium.

### B. Crossover from destructive QI to ATS in the GAL-I system

We now employ the SDM used in Sec. II B to make a detailed analysis on the QI effect in the GAL-I system. For  $\Delta_3$  much larger than  $\gamma_{ij}$ ,  $\Gamma_{ij}$ ,  $\Omega_p$ , and  $\Omega_c$ , Eq. (14) is reduced to  $K = \omega/c + \tilde{\kappa}_{23}(\omega + i\gamma_{41})/[(\omega + i\gamma_{21})(\omega + i\gamma_{41}) - |\Omega_c|^2]$  with  $\tilde{\kappa}_{23} = \kappa_{23}\Omega_p\sigma_{31}^{(0)*}/\Delta_3$ , which can be written as the form

$$K(\omega) = \frac{\omega}{c} + \tilde{\kappa}_{23} \frac{\omega + i\gamma_{41}}{(\omega - \omega_+)(\omega - \omega_-)}. \quad (15)$$

Here  $\omega_{\pm} = -i(\gamma_{21} + \gamma_{41})/2 \pm [|\Omega_c|^2 - |\Omega_{\text{ref}}|^2]^{1/2}$  with  $\Omega_{\text{ref}} = |\gamma_{21} - \gamma_{41}|/2$  the reference half Rabi frequency. The gain spectrum  $-\text{Im}(K)$  can be decomposed into three different regions.

(i). *Weak control field region* ( $|\Omega_c| < \Omega_{\text{ref}}$ ): Eq. (15) can be decomposed into

$$K(\omega) = \frac{\omega}{c} + \tilde{\kappa}_{23} \left( \frac{A_+}{\omega - \omega_+} + \frac{A_-}{\omega - \omega_-} \right), \quad (16)$$

where  $A_{\pm} = \pm(\omega_{\pm} + i\gamma_{41})/(\omega_+ - \omega_-)$ . Since  $\text{Re}(\omega_{\pm}) = \text{Im}(A_{\pm}) = 0$ , we have

$$-\text{Im}(K) = -\tilde{\kappa}_{23} \left( \frac{B_+}{\omega^2 + \delta_+^2} + \frac{B_-}{\omega^2 + \delta_-^2} \right) = -L_+ - L_-, \quad (17)$$

with  $\delta_{\pm} = \text{Im}(\omega_{\pm})$ ,  $B_{\pm} = A_{\pm}\delta_{\pm}$ , and  $L_{\pm} = \tilde{\kappa}_{23}B_{\pm}/(\omega^2 + \delta_{\pm}^2)$ . Thus the signal-field gain profile comprises two Lorentzian centered at the origin ( $\omega = 0$ ).

Fig. 5(a) shows the profile of  $-L_+$ , which is a positive single peak (red dashed line), and  $-L_-$ , which is a negative single peak (black dash-dotted line). When plotting the figure  $\Omega_c = 0.2\Gamma$  is chosen and the other system parameters are the same as in Fig. 4(a). The superposition of  $-L_+$  and  $-L_-$  gives the profile of  $-\text{Im}(K)$  (blue solid line), which has a gain doublet with a gain window opened near  $\omega = 0$ . We see that there exists a destructive QI in the GAL-I system, reflecting by the sum of the positive  $-L_+$  and the negative  $-L_-$ , very similar to the destructive QI in the ladder-I type EIT system found recently [32].

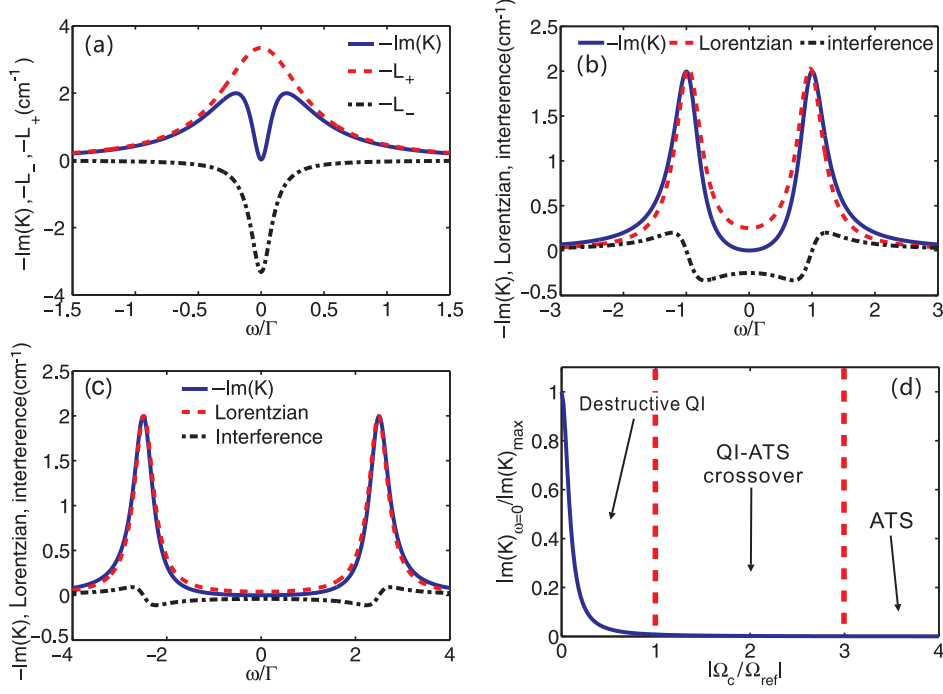


FIG. 5. (Color online) (a) Gain spectrum  $-\text{Im}(K)$  in the weak control field region ( $\Omega_c = 0.2\Gamma < \Omega_{\text{ref}}$ ) as a function of  $\omega/\Gamma$ . Red dashed line:  $-L_+$ ; black dashed-dotted line:  $-L_-$ ; blue solid line:  $-\text{Im}(K)$ . (b) Gain spectrum in the intermediate control field region ( $\Omega_c = 1.0\Gamma < \Omega_{\text{ref}}$ ). Red dashed line: two Lorentzian terms; black dashed-dotted line: destructive QI term; blue solid line:  $-\text{Im}(K)$ . (c) Gain spectrum in the strong control field region ( $\Omega_c = 2.5\Gamma > \Omega_{\text{ref}}$ ). Red dashed line: two Lorentzian terms; black dashed-dotted line: destructive QI term; blue solid line:  $-\text{Im}(K)$ . (d) The “phase diagram” of  $\text{Im}(K)_{\omega=0}/\text{Im}(K)_{\text{max}}$  as a function of  $|\Omega_c/\Omega_{\text{ref}}|$  illustrating the crossover from destructive QI to ATS in the GAL-I system. Three regions (i.e. destructive QI region, QI-ATS crossover region, and ATS region) are divided by two vertical dashed lines.

(ii). *Intermediate control field region* ( $|\Omega_c| > \Omega_{\text{ref}}$ ): In this region  $\text{Re}(\omega_{\pm}) \neq 0$ , we obtain

$$-\text{Im}(K) = \frac{\tilde{\kappa}_{23}}{2} \left\{ \frac{W}{(\omega - \delta)^2 + W^2} + \frac{W}{(\omega + \delta)^2 + W^2} + \frac{g}{\delta} \left[ \frac{\omega - \delta}{(\omega - \delta)^2 + W^2} - \frac{\omega + \delta}{(\omega + \delta)^2 + W^2} \right] \right\}, \quad (18)$$

with  $W = (\gamma_{21} + \gamma_{41})/2$ ,  $\delta = [4|\Omega_c|^2 - (\gamma_{21} - \gamma_{41})^2]^{1/2}/2$ , and  $g = (\gamma_{21} - \gamma_{41})/2$ . The first two terms (Lorentzian terms) in bracket of Eq. (18) are the net contribution by the gain resonance from two different channels corresponding to the two dressed states (state  $|2\rangle$  and  $|4\rangle$ ). The terms proportional to  $g$  are clearly interference ones. The interference is governed

by the parameter  $g$  and it is destructive (constructive) if  $g > 0$  ( $g < 0$ ). Because in the GAL-I system  $\gamma_{21}$  is much smaller than  $\gamma_{41}$ ,  $g$  is always positive. Thus the QI induced by the control field is destructive.

Fig. 5(b) shows the gain spectrum  $-\text{Im}(K)$  in the intermediate control field region. The red dashed line is for the two positive Lorentzian terms; the black dashed-dotted line is for the negative QI term. We see that in this region a gain doublet appears in the gain spectrum (blue solid line), which is the result of the superposition of the two positive Lorentzian terms and the negative (thus destructive) QI term. When plotting the figure, the system parameters used are the same as those in Fig. 5(a) except  $\Omega_c = 1.0\Gamma$ .

(iii). *Large control field region* ( $|\Omega_c| \gg \Omega_{\text{ref}}$ ): In this case, the quantum interference strength  $g/\delta$  in Eq. (18) is very weak (i.e.  $g/\delta \approx 0$ ), and hence  $\text{Im}(K)$  can be simplified to  $-\text{Im}(K) = (\tilde{\kappa}_{23}/2) \{W/[(\omega - \delta)^2 + W^2] + W/[(\omega + \delta)^2 + W^2]\}$ . Shown in Fig. 5(c) is the signal-field gain spectrum as a function of  $\omega/\Gamma$  in the large control field region ( $\Omega_c = 2.5\Gamma$ ). The red dashed line is the contribution by the sum of the two positive Lorentzian terms. The contribution of very small interference terms are also plotted as the black dotted-dashed line, which is negative and thus destructive. The blue solid line is for  $-\text{Im}(K)$ . Obviously, the phenomenon found in this case belongs to ATS because the gain window is wide and mainly due to the contribution of two Lorentzian terms.

In Fig. 5(d) we show the “phase diagram” of the system, which reflects the crossover from the destructive QI effect to the ATS in the GAL-I system, by taking  $\text{Im}(K)_{\omega=0}/\text{Im}(K)_{\text{max}}$  as a function of  $|\Omega_c/\Omega_{\text{ref}}|$ . We see that the phase diagram can also be divided into three regions, i.e. the destructive QI region (weak control field region), the QI-ATS crossover region (intermediate control field region), and the ATS region (large control field region), similar to those found in EIT systems for slow lights [26–36].

The physical reason for the occurrence of the QI here (i.e. the gain doublet in the gain spectrum in Fig. 4(a)) can also be explained by the existence of a dark state in the system. From the system Hamiltonian we obtain an eigenstate

$$|\psi\rangle = \left[1 + \frac{|\Omega_s|^2 d_4}{(|\Omega_c|^2 - d_2 d_4) d_3}\right] |1\rangle - \frac{\Omega_p \Omega_s d_4}{(|\Omega_c|^2 - d_2 d_4) d_3} |2\rangle - \frac{\Omega_p}{d_3} |3\rangle + \frac{\Omega_p \Omega_c^* \Omega_s}{(|\Omega_c|^2 - d_2 d_4) d_3} |4\rangle, \quad (19)$$

where  $d_2 = \Delta_2 + i\Gamma_2$ ,  $d_3 = \Delta_3 + i\Gamma_3$ ,  $d_4 = \Delta_4 + i\Gamma_4$ . For large  $\Delta_3$  and  $\Omega_c$  and for small  $\Delta_2$  and  $\Delta_4$ , the eigenstate (19) reduces to  $|\psi\rangle \approx |1\rangle - (\Omega_p/\Delta_3)|3\rangle + [\Omega_p \Omega_c^* \Omega_s / (|\Omega_c|^2 \Delta_3)] |4\rangle$ . Because state  $|2\rangle$  is not involved,  $|\psi\rangle$  is a “dark state” with zero eigenvalue, which is resulted from

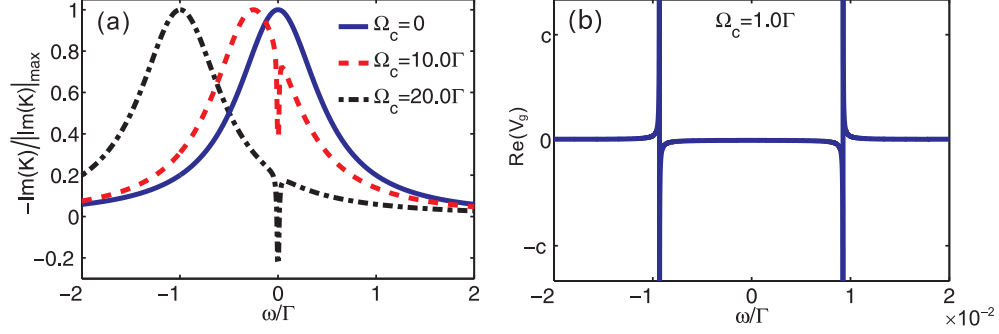


FIG. 6. (Color online) (a) Gain spectrum of the signal field,  $-\text{Im}(K)$ , as a function of  $\omega/\Gamma$  and  $\Omega_c$  for the GAL-II system. For  $\Omega_c = 0$  it has only a large single peak centered at  $\omega = 0$  (blue solid line). For  $\Omega_c = 10.0\Gamma$ , a very narrow gain doublet (dip) is opened around  $\omega = 0$  and the large single peak moves to the left (red dashed line). For  $\Omega_c = 20.0\Gamma$ , the gain doublet still keeps to exist near at  $\omega = 0$  but the the large single peak moves further to the left (black dotted-dashed line). (b) Group velocity  $\text{Re}(V_g)$  of the signal field of the GAL-II system as a function of  $\omega/\Gamma$  for  $\Omega_c = 1.0\Gamma$ .

the interference between the two quantum transition passages from  $|3\rangle \rightarrow |2\rangle$  and  $|4\rangle \rightarrow |2\rangle$ . The outcome of such quantum interference is appearance of the gain doublet in the gain spectrum of the signal field.

#### IV. AUTLER-TOWNES SPLITTING IN THE GAL-II SYSTEM

Finally, we consider the GAL-II system (Fig. 1(c)). Under EDA and RWA, the Hamiltonian of the GAL-II system in interaction picture is  $\hat{\mathcal{H}} = -\hbar[\sum_{j=1}^4 \Delta_j |j\rangle\langle j| + (\Omega_p |3\rangle\langle 1| + \Omega_c |3\rangle\langle 2| + \Omega_s |2\rangle\langle 4| + \text{h.c.})]$ . The Bloch equations for the GAL-II system can be obtained from those of the GAL-I system given in Appendix B, by using the exchange of  $\Omega_s \rightleftharpoons \Omega_c$ . Under SVEA, the Maxwell equation of the signal field reduces to  $i[\partial/\partial z + (1/c)\partial/\partial t] \Omega_s + \kappa_{24} \sigma_{42} = 0$ , with  $\kappa_{24} = \mathcal{N}_a \omega_s |\mathbf{p}_{42}|^2 / (2\hbar \varepsilon_0 c)$ . The base state of the system is presented in Appendix C.

It is easy to obtain the linear dispersion relation of the system

$$K(\omega) = \frac{\omega}{c} + \kappa_{24} \frac{(\omega + d_{41}) \Omega_c \sigma_{32}^{(0)*} + \Omega_p^* \Omega_c \sigma_{21}^{(0)} + D_p (\sigma_{44}^{(0)} - \sigma_{22}^{(0)})}{D_p (\omega + d_{42}) + |\Omega_c|^2 (\omega + d_{41})}, \quad (20)$$

with  $D_p = |\Omega_p|^2 - (\omega + d_{41})(\omega + d_{43})$  and  $D_c = |\Omega_c|^2 - (\omega + d_{42})(\omega + d_{43})$ .

Shown in Fig. 6(a) is the signal-field gain spectrum,  $-\text{Im}(K)$ , as a function of  $\omega/\Gamma$  for



different  $\Omega_c$ . One sees that for  $\Omega_c = 0$  the gain spectrum has only a single peak centered at  $\omega = 0$  (blue solid line); Increasing the value of  $\Omega_c$  to  $10.0\Gamma$ , a gain doublet (dip) opens around  $\omega = 0$  with the single peak moves to the left (red dashed line); Increasing  $\Omega_c$  further to  $20.0\Gamma$ , the gain doublet still keeps near at  $\omega = 0$  but the single peak moves further to the left (black dotted-dashed line). When drawing the figure, the four atomic states and the system parameters used are the same as those for the GAL-I system (see the last section). The condition for the appearance of the gain doublet in the GAL-II system is  $|\Omega_c|^2 > \Delta_3\gamma_{42}$ .

Comparing Fig. 6(a) with Fig. 2(a) and Fig. 4(a), we find that there are obvious differences between them. First, the gain doublet is not opened near at  $\omega = 0$ ; Second, the gain doublet is very narrow even for a very large control field. The physical reason is that for the large control field the base state of the GAL-II system has very different property from the GAN and GAL-I systems. In addition, there is no QI effect in the GAL-II system, as shown below.

Fig. 6(b) shows the group velocity of the signal field  $\text{Re}(V_g)$  in the GAL-I system as a function of  $\omega/\Gamma$  for  $\Omega_c = 1.0\Gamma$ . One sees that, as in the GAN and GAL-I systems, the GAL-II system can also have subluminal and superluminal group velocities.

We can also make an analysis of the QI character in the GAL-II system by using the SDM. For  $\Delta_3$  larger than  $\gamma_{ij}$ ,  $\Gamma_{ij}$ ,  $\Omega_p$ ,  $\Omega_c$ , Eq. (20) reduces to the form  $\tilde{K}(\omega) = \omega/c + \tilde{\kappa}_{24}(\omega + i\tilde{\gamma}_{41}/2)/[(\omega + i\gamma_{41})(\omega + i\gamma_{42} + |\Omega_c|^2/\Delta_3)]$ , which can be written as

$$K(\omega) = \frac{\omega}{c} + \tilde{\kappa}_{24} \frac{\omega + i\tilde{\gamma}_{41}/2}{(\omega - \omega_+)(\omega - \omega_-)}, \quad (21)$$

with  $\tilde{\kappa}_{24} = \kappa_{24}\sigma_{44}^{(0)}$ ,  $\tilde{\gamma}_{41} = \gamma_{41} + \gamma_{41}/(|\Omega_c|^2 + 1)$ ,  $\omega_+ = -i\gamma_{41}$ , and  $\omega_- = -i\gamma_{42} - |\Omega_c|^2/\Delta_3$ . Equation (21) is different that for GAL-I system because now  $\omega_+$  is purely imaginary, which brings some different features for the GAL-II system. First, the two peaks in the signal-field gain spectrum  $-\text{Im}(K)$  for non-zero  $\Omega_c$  becomes asymmetric (see the red dashed and black dotted-dashed lines in Fig. 6(a)) because the no real part exists for  $\omega_+$  but the real part of  $\omega_-$  is proportional to  $|\Omega_c|^2$ . This fact also explains why the small peak on the right (the large peak on the left) of the gain dip locates at  $\omega = 0$  (at  $\omega = -|\Omega_c|^2/\Delta_3$ ). Second, different from the GAN and GAL-I systems, in the GAL-II system  $\omega_-$  is always complex, so one cannot set up a parameter  $\Omega_{\text{ref}}$  to divide the system into three control field regions.

It is easy to show that the gain spectrum of the GAL-II system can be decomposed into

$$-\text{Im}(K) = \frac{\tilde{\kappa}_{24}}{2} \left\{ \frac{f_1 W_1}{\omega^2 + W_1^2} + \frac{f_2 W_2}{(\omega + R_2)^2 + W_2^2} + \frac{g}{\delta} \left[ \frac{\omega}{\omega^2 + W_1^2} - \frac{\omega + R_2}{(\omega + R_2)^2 + W_2^2} \right] \right\}, \quad (22)$$

with  $W_1 = \gamma_{41}$ ,  $W_2 = \gamma_{42}$ ,  $R_2 = |\Omega_c|^2/\Delta_3$ ,  $f_1 = [-2W_1(W_2 - W_1) + \tilde{\gamma}_{41}(W_2 - W_1)]/\delta$ ,  $f_2 = [2R_2^2 + 2W_2(W_2 - W_1) - \tilde{\gamma}_{41}(W_2 - W_1)]/\delta$ ,  $g = R_2(2W_1 - \tilde{\gamma}_{41})$ , and  $\delta = R_2^2 + (W_2 - W_1)^2$ . The first two terms in the bracket of Eq. (22) are two Lorentzian terms. The following terms are proportional to  $g/\delta$ . By a simple estimation one obtains  $g/\delta \simeq -\gamma_{41}/(2\Delta_3)$ , which is negligibly small. So the gain spectrum has only two Lorentzian terms and no interference term, we thus conclude that there is no QI in GAL-II system and hence the system displays only an ATS effect.

The GAL-II system has additional properties absent in the GAN and GAL-I systems. For example, it can become absorptive for a large control field. This point has already been shown in Fig. 6(a), where the gain dip opened in the black dotted-dashed line becomes deep enough so that  $-\text{Im}(K)$  becomes negative. The physical reason is that for a large  $\Omega_c$  the population is mainly in the state  $|4\rangle$ , resulting in a significant absorption of the signal field.

Note that in addition to the level configuration indicated in the Sec. III the GAL-I and GAL-II systems can also be realized by using the following level configuration, i.e.  $|1\rangle = |5^2S_{1/2}, F = 1, m_F = -1\rangle$ ,  $|2\rangle = |5^2S_{1/2}, F = 2, m_F = 0\rangle$ ,  $|3\rangle = |5^2P_{1/2}, F = 2, m_F = 0\rangle$ , and  $|4\rangle = |5^2S_{3/2}, F = 1, m_F = 0\rangle$ . In this case, the transition between  $|1\rangle$  and  $|3\rangle$  is a single-photon one, and the field coupled to  $|2\rangle$  and  $|4\rangle$  is a microwave or radiation-frequency field [40].

## V. DISCUSSION AND SUMMARY

From Sec. II to Sec. IV, we have analyzed the QI characters in the GAN, GAL-I, and GAL-II systems. For comparison, in Table I we have summarized the main results obtained for different systems. If in the table there is ‘‘Yes’’ in the same line for both QI and ATS, an QI-ATS crossover also exists in the system.

One may question possible influence resulted from Doppler effect resulted from the thermal motion of the atoms, which is omitted in the above discussions. When the Doppler effect is considered, all calculations for the GAN, GAL-I and GAL-II systems can still be

TABLE I. QI characters of fast-light media

System	Gain-doublet condition	QI effect	ATS
GAN	$ \Omega_c ^2 > \frac{\kappa_{23} \Omega_p ^2\gamma_{41}}{\Delta_3^2}$	Constructive	Yes
GAL-I	$ \Omega_c ^2 > \frac{\kappa_{23} \Omega_p ^2\gamma_{41}}{\Delta_3^2}$	Destructive	Yes
GAL-II	$ \Omega_c ^2 > \Delta_3\gamma_{42}$	No	Yes

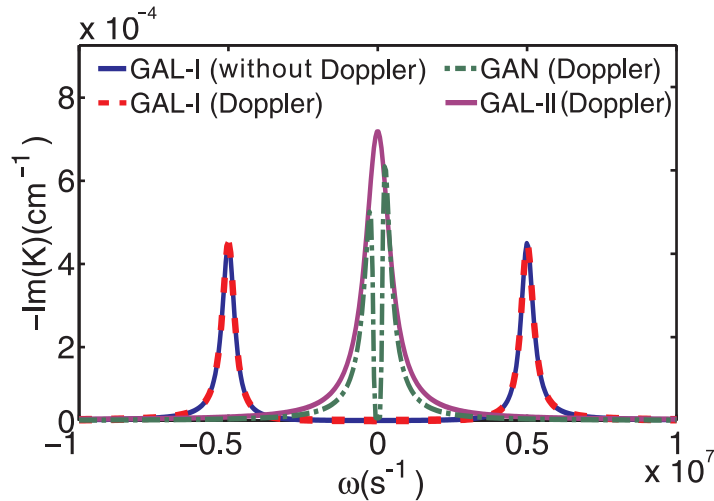


FIG. 7. (Color online) Gain spectrum  $-\text{Im}(K)$  as functions of  $\omega$  for  $\Omega_c = 5.0\Gamma$ . The red dashed line (blue solid line) is for the GAL-I system with (without) Doppler effect. The green dashed-dotted line is for GAN system with Doppler effect. The purple solid line is for the GAL-II system with Doppler effect, which has been multiplied by  $1/30$ .

carried out. As an example, in Appendix D we present the result for the GAL-I system. The conclusion is that, in the GAL-I system the QI and the crossover from the QI to ATS are nearly the same as in the case without Doppler effect if an experimental geometry of cancelling Doppler effect is adopted.

To show the difference between the three fast-light media with Doppler effect, in Fig. 7 we show the gain spectrum  $-\text{Im}(K)$  of the GAN, GAL-I and GAL-II systems as functions of  $\omega$  for  $\Omega_c = 5.0\Gamma$  when Doppler broadening is taken into account. In the figure, the red dashed line (blue solid line) is for the GAL-I system with (without) Doppler effect; the green dashed-dotted line is for GAN system with Doppler effect; the purple solid line is for the GAL-II system with Doppler effect, which has been multiplied by  $1/30$  for display in the figure. We see that for the GAL-I system there is almost no difference between the situations

with and without Doppler effect. However, it can be shown that for the GAN and the GAL-II systems, the QI characters with Doppler effect have some differences in comparison with the case without Doppler effect. Especially, when the Doppler effect is present the width of the gain doublet for the GAN system becomes very narrow and the two peaks become asymmetric and are amplified (green dashed-dotted line).

In conclusion, in this article we have made a systematic analysis on the QI effect in several fast-light media by using an extended spectrum-decomposition method. We have shown that such fast-light media are capable of not only completely eliminating the absorption but also suppressing the gain of signal field, and hence provide the possibility to realize a stable long-distance propagation of the signal field with a superluminal velocity. We have found that there is a destructive (constructive) QI effect in GAL-I (GAN) system, but no QI in the GAL-II system. We further found that a crossover from destructive (constructive) QI to Autler-Townes splitting may happen for the GAL-I (GAN) system when the control field of the system is manipulated.

The fast-light media presented here may have giant Kerr nonlinearities, as demonstrated in Refs. [4, 17–20, 22]. The fast, all-Optical, zero to  $\pi$  continuously controllable phase gates based on such media have been realized experimentally in Ref. [21]. The theoretical method presented here can be applied to other multi-level atoms, or other physical systems (e.g. molecules, quantum dots, nitrogen-valence centers in diamond, and rare-earth ions in crystals, etc.) and the results obtained can help to deepen the understanding of fast-light physics and fast-light spectroscopy and may have promising applications in optical and quantum information processing and transmission, including the enhancement of optical Kerr effect and the realization of light storage and retrieval by means of fast light media [45].

## ACKNOWLEDGMENTS

This work was supported by the NSF-China under Grants No. 11174080 and No. 11474099.

## Appendix A: Bloch equations for the N system

The explicit expression of the Bloch Eq. (1) is given by

$$i \frac{\partial}{\partial t} \sigma_{11} - i\Gamma_{13}\sigma_{33} - i\Gamma_{14}\sigma_{44} + \Omega_p^* \sigma_{31} - \Omega_p \sigma_{31}^* = 0, \quad (\text{A1a})$$

$$i \frac{\partial}{\partial t} \sigma_{22} - i\Gamma_{23}\sigma_{33} - i\Gamma_{24}\sigma_{44} + \Omega_s^* \sigma_{32} - \Omega_s \sigma_{32}^* + \Omega_c^* \sigma_{42} - \Omega_c \sigma_{42}^* = 0, \quad (\text{A1b})$$

$$i \left( \frac{\partial}{\partial t} + \Gamma_3 \right) \sigma_{33} + \Omega_s \sigma_{32}^* + \Omega_p \sigma_{31}^* - \Omega_s^* \sigma_{32} - \Omega_p^* \sigma_{31} = 0, \quad (\text{A1c})$$

$$i \left( \frac{\partial}{\partial t} + \Gamma_4 \right) \sigma_{44} + \Omega_c \sigma_{42}^* - \Omega_c^* \sigma_{42} = 0, \quad (\text{A1d})$$

for the diagonal matrix elements, and

$$\left( i \frac{\partial}{\partial t} + d_{21} \right) \sigma_{21} + \Omega_c^* \sigma_{41} + \Omega_s^* \sigma_{31} - \Omega_p \sigma_{32}^* = 0, \quad (\text{A2a})$$

$$\left( i \frac{\partial}{\partial t} + d_{31} \right) \sigma_{31} + \Omega_p (\sigma_{11} - \sigma_{33}) + \Omega_s \sigma_{21} = 0, \quad (\text{A2b})$$

$$\left( i \frac{\partial}{\partial t} + d_{32} \right) \sigma_{32} + \Omega_p \sigma_{21}^* + \Omega_s (\sigma_{22} - \sigma_{33}) - \Omega_c \sigma_{43}^* = 0, \quad (\text{A2c})$$

$$\left( i \frac{\partial}{\partial t} + d_{41} \right) \sigma_{41} + \Omega_c \sigma_{21} - \Omega_p \sigma_{43} = 0, \quad (\text{A2d})$$

$$\left( i \frac{\partial}{\partial t} + d_{42} \right) \sigma_{42} + \Omega_c (\sigma_{22} - \sigma_{44}) - \Omega_s \sigma_{43} = 0, \quad (\text{A2e})$$

$$\left( i \frac{\partial}{\partial t} + d_{43} \right) \sigma_{43} + \Omega_c \sigma_{32}^* - \Omega_p^* \sigma_{41} - \Omega_s^* \sigma_{42} = 0, \quad (\text{A2f})$$

for the off-diagonal matrix elements, where  $d_{21} = \Delta_2 + i\gamma_{21}$ ,  $d_{31} = \Delta_3 + i\gamma_{31}$ ,  $d_{32} = \Delta_3 - \Delta_2 + i\gamma_{32}$ ,  $d_{41} = \Delta_4 + i\gamma_{41}$ ,  $d_{42} = \Delta_4 - \Delta_2 + i\gamma_{42}$ ,  $d_{43} = \Delta_4 - \Delta_3 + i\gamma_{43}$  with  $\gamma_{jl} = (\Gamma_j + \Gamma_l)/2 + \gamma_{jl}^{\text{dep}}$ . Here  $\Gamma_j = \sum_{l < j} \Gamma_{lj}$  with  $\Gamma_{jl}$  ( $\gamma_{jl}^{\text{dep}}$ ) the population decay rate (dephasing rate) from the level  $|l\rangle$  and  $|j\rangle$  ( $j, l = 1-4$ ).

## Appendix B: Bloch equations for the GAL-I system

The Bloch equations of the GAL-I system read

$$i \frac{\partial}{\partial t} \sigma_{11} - i\Gamma_{13}\sigma_{33} - i\Gamma_{14}\sigma_{44} + \Omega_p^* \sigma_{31} - \Omega_p \sigma_{31}^* = 0, \quad (\text{B1a})$$

$$i \left( \frac{\partial}{\partial t} + \Gamma_{42} \right) \sigma_{22} - i\Gamma_{23}\sigma_{33} + \Omega_s^* \sigma_{32} - \Omega_s \sigma_{32}^* + \Omega_c^* \sigma_{42} - \Omega_c \sigma_{42}^* = 0, \quad (\text{B1b})$$

$$i \left( \frac{\partial}{\partial t} + \Gamma_3 \right) \sigma_{33} + \Omega_s \sigma_{32}^* + \Omega_p \sigma_{31}^* - \Omega_s^* \sigma_{32} - \Omega_p^* \sigma_{31} = 0, \quad (\text{B1c})$$

$$i \left( \frac{\partial}{\partial t} + \Gamma_4 \right) \sigma_{44} - i\Gamma_{42}\sigma_{22} + \Omega_c \sigma_{42}^* - \Omega_c^* \sigma_{42} = 0, \quad (\text{B1d})$$

for the off-diagonal matrix elements, and

$$\left( i \frac{\partial}{\partial t} + d_{21} \right) \sigma_{21} + \Omega_c^* \sigma_{41} + \Omega_s^* \sigma_{31} - \Omega_p \sigma_{32}^* = 0, \quad (\text{B2a})$$

$$\left( i \frac{\partial}{\partial t} + d_{31} \right) \sigma_{31} + \Omega_p (\sigma_{11} - \sigma_{33}) + \Omega_s \sigma_{21} = 0, \quad (\text{B2b})$$

$$\left( i \frac{\partial}{\partial t} + d_{32} \right) \sigma_{32} + \Omega_p \sigma_{21}^* + \Omega_s (\sigma_{22} - \sigma_{33}) - \Omega_c \sigma_{43}^* = 0, \quad (\text{B2c})$$

$$\left( i \frac{\partial}{\partial t} + d_{41} \right) \sigma_{41} + \Omega_c \sigma_{21} - \Omega_p \sigma_{43} = 0, \quad (\text{B2d})$$

$$\left( i \frac{\partial}{\partial t} + d_{42} \right) \sigma_{42} + \Omega_c (\sigma_{22} - \sigma_{44}) - \Omega_s \sigma_{43} = 0, \quad (\text{B2e})$$

$$\left( i \frac{\partial}{\partial t} + d_{43} \right) \sigma_{43} + \Omega_c \sigma_{32}^* - \Omega_p^* \sigma_{41} - \Omega_s^* \sigma_{42} = 0, \quad (\text{B2f})$$

for the off-diagonal matrix elements, where  $d_{21} = \Delta_2 - \Delta_1 + i\gamma_{21}$ ,  $d_{31} = \Delta_3 - \Delta_1 + i\gamma_{31}$ ,  $d_{32} = \Delta_3 - \Delta_2 + i\gamma_{32}$ ,  $d_{41} = \Delta_4 - \Delta_1 + i\gamma_{41}$ ,  $d_{42} = \Delta_4 - \Delta_2 + i\gamma_{42}$ , and  $d_{43} = \Delta_4 - \Delta_3 + i\gamma_{43}$ .

The base state of the GAL-I system (i.e. the steady-state solution of the MB Eqs. (B1), (B2), and (12) for  $\Omega_s = 0$ ) is given by

$$\sigma_{11}^{(0)} = \frac{\Gamma_{14}(|\Omega_c|^2 + \Gamma_{42}X_{42})(\Gamma_3 X_{31} + |\Omega_p|^2)}{D}, \quad (\text{B3a})$$

$$\sigma_{22}^{(0)} = \frac{\Gamma_{23}|\Omega_p|^2(\Gamma_4 X_{42} + |\Omega_c|^2)}{D}, \quad (\text{B3b})$$

$$\sigma_{33}^{(0)} = \frac{\Gamma_{14}(|\Omega_c|^2 + \Gamma_{42}X_{42})|\Omega_p|^2}{D}, \quad (\text{B3c})$$

$$\sigma_{44}^{(0)} = \frac{\Gamma_{23}(|\Omega_c|^2 + \Gamma_{42}X_{42})|\Omega_p|^2}{D}, \quad (\text{B3d})$$

$$\sigma_{31}^{(0)} = -\frac{\Omega_p}{d_{31}} \frac{\Gamma_{14}\Gamma_3 X_{31}(|\Omega_c|^2 + \Gamma_{42}X_{42})}{D}, \quad (\text{B3e})$$

$$\sigma_{42}^{(0)} = -\frac{\Omega_c}{d_{42}} \frac{\Gamma_{23}(\Gamma_4 - \Gamma_{42})X_{42}|\Omega_p|^2}{D}, \quad (\text{B3f})$$

and other  $\sigma_{jl}^{(0)} = 0$ . Here we have defined  $X_{31} = |d_{31}|^2/(2\gamma_{31})$ ,  $X_{42} = |d_{42}|^2/(2\gamma_{42})$  and  $D = \Gamma_{14}(|\Omega_c|^2 + \Gamma_{42}X_{42})(\Gamma_3X_{31} + 2|\Omega_p|^2) + \Gamma_{23}|\Omega_p|^2[(\Gamma_4 - \Gamma_{42})X_{42} + 2(|\Omega_c|^2 + \Gamma_{42}X_{42})]$ . For large  $\Delta_3$ , the base state solution is simplified into  $\sigma_{11}^{(0)} \approx 1$ ,  $\sigma_{31}^{(0)} \approx -\Omega_p/d_{31}$ , and all other  $\sigma_{jl}^{(0)} \approx 0$ .

### Appendix C: Base state solution of the GAL-II system

The base state solution of the GAL-II system is

$$\sigma_{22}^{(0)} = \frac{\alpha_{12}\alpha_{23} - \alpha_{22}\alpha_{13}}{\alpha_{11}\alpha_{22} - \alpha_{12}\alpha_{21}}, \quad (\text{C1a})$$

$$\sigma_{33}^{(0)} = \frac{\alpha_{13}\alpha_{21} - \alpha_{11}\alpha_{23}}{\alpha_{11}\alpha_{22} - \alpha_{12}\alpha_{21}}, \quad (\text{C1b})$$

$$\sigma_{44}^{(0)} = \frac{\Gamma_{42}}{\Gamma_4}\sigma_{22}^{(0)}, \quad (\text{C1c})$$

$$\sigma_{11}^{(0)} = 1 - \sigma_{22}^{(0)} - \sigma_{33}^{(0)} - \sigma_{44}^{(0)}, \quad (\text{C1d})$$

$$\sigma_{21}^{(0)} = \frac{\Omega_p\Omega_c^* \left[ d_{32}^* - \left( \frac{\Gamma_{42}}{\Gamma_4}d_{32}^* + d_{31} \right) \sigma_{22}^{(0)} + (d_{31} - 2d_{32}^*)\sigma_{33}^{(0)} \right]}{B}, \quad (\text{C1e})$$

$$\sigma_{31}^{(0)} = \frac{-\Omega_c\sigma_{21}^{(0)} - \Omega_p(\sigma_{11}^{(0)} - \sigma_{33}^{(0)})}{d_{31}}, \quad (\text{C1f})$$

$$\sigma_{32}^{(0)} = \frac{-\Omega_p\sigma_{21}^{(0)*} - \Omega_c(\sigma_{22}^{(0)} - \sigma_{33}^{(0)})}{d_{32}}, \quad (\text{C1g})$$

with

$$B = d_{21}d_{32}^*d_{31} + d_{31}|\Omega_p|^2 - d_{32}^*|\Omega_c|^2, \quad (\text{C2a})$$

$$\begin{aligned} \alpha_{11} = & -i\Gamma_{42} + |\Omega_p|^2|\Omega_c|^2 \left( 1 + \frac{\Gamma_{42}}{\Gamma_4} \right) \left( \frac{d_{32}^*}{Bd_{31}} - \frac{d_{32}}{B^*d_{31}^*} \right) \\ & + |\Omega_p|^2|\Omega_c|^2 \left( \frac{1}{B} - \frac{1}{B^*} \right) + |\Omega_p|^2 \left( 1 + \frac{\Gamma_{42}}{\Gamma_4} \right) \left( \frac{2i\gamma_{31}}{|d_{31}|^2} \right), \end{aligned} \quad (\text{C2b})$$

$$\begin{aligned} \alpha_{12} = & -i\Gamma_{13} + 2|\Omega_p|^2 \left( \frac{1}{d_{31}} - \frac{1}{d_{31}^*} \right) + 2|\Omega_p|^2|\Omega_c|^2 \left( 1 + \frac{\Gamma_{42}}{\Gamma_4} \right) \left( \frac{d_{32}^*}{Bd_{31}} - \frac{d_{32}}{B^*d_{31}^*} \right) \\ & + |\Omega_p|^2|\Omega_c|^2 \left( \frac{1}{B^*} - \frac{1}{B} \right), \end{aligned} \quad (\text{C2c})$$

$$\alpha_{13} = |\Omega_p|^2|\Omega_c|^2 \left( \frac{d_{32}}{B^*d_{31}^*} - \frac{d_{32}^*}{Bd_{31}} \right) + |\Omega_p|^2 \left( \frac{1}{d_{31}^*} - \frac{1}{d_{31}} \right), \quad (\text{C2d})$$

and

$$\begin{aligned} \alpha_{21} = & i\Gamma_{42} + |\Omega_p|^2|\Omega_c|^2 \left(1 + \frac{\Gamma_{42}}{\Gamma_4}\right) \left(\frac{1}{B^*} - \frac{1}{B}\right) + |\Omega_p|^2|\Omega_c|^2 \left(\frac{d_{31}^*}{B^*d_{32}} - \frac{d_{31}}{Bd_{32}^*}\right) \\ & + |\Omega_c|^2 \left(\frac{1}{d_{32}^*} - \frac{1}{d_{32}}\right), \end{aligned} \quad (\text{C3a})$$

$$\begin{aligned} \alpha_{22} = & -i\Gamma_{23} + 2|\Omega_p|^2|\Omega_c|^2 \left(\frac{1}{B^*} - \frac{1}{B}\right) + |\Omega_p|^2|\Omega_c|^2 \left(\frac{d_{31}}{Bd_{32}^*} - \frac{d_{31}^*}{B^*d_{32}}\right) \\ & + |\Omega_c|^2 \left(\frac{1}{d_{32}} - \frac{1}{d_{32}^*}\right), \end{aligned} \quad (\text{C3b})$$

$$\alpha_{23} = |\Omega_p|^2|\Omega_c|^2 \left(\frac{1}{B} - \frac{1}{B^*}\right). \quad (\text{C3c})$$

#### Appendix D: QI effect in the GAL-I system with Doppler effect

When the Doppler effect is considered, the linear dispersion relation of the GAL-I system reads

$$K(\omega) = \frac{\omega}{c} + \tilde{\kappa}_{23} \int_{-\infty}^{\infty} f(v) \frac{\omega + d_{41}}{(\omega + d_{21})(\omega + d_{41}) - |\Omega_c|^2} dv \quad (\text{D1})$$

with  $d_{41} = \Delta_4 + i\gamma_{41} - (k_p - k_c - k_s)v$ ,  $d_{21} = \Delta_2 + i\gamma_{21} - (k_p - k_s)v$ ,  $f(v)$  is Maxwell velocity distribution function. To show clearly whether the QI still keeps or not, as done in Refs. [41–43] we replace the Maxwell velocity distribution function by a modified Lorentzian velocity distribution  $f(v) = v_T/[\sqrt{\pi}(v^2 + v_T^2)]$ , where  $v_T = \sqrt{2k_B T/M}$  is the most probable speed at temperature  $T$  with  $k_B$  the Boltzmann constant and  $M$  the particle mass. We assume that all three light fields are incident in the same (i.e.  $z$ ) direction (i.e. an “almost Doppler-free” geometry [44]). Since in this situation  $k_p - k_s - k_s \approx 0$ , one has  $d_{41} \approx \Delta_4 + i\gamma_{41}$  and hence the integrand in the integral of Eq. (D1) can be simplified largely. By using the residue theorem [41–43], one can carry out the integral analytically, yielding the result  $K(\omega) = \omega/c + \tilde{\kappa}_{23}\sqrt{\pi}(\omega + i\gamma_{41})/[(\omega + i\gamma_{21} + i\Delta\omega_D)(\omega + i\gamma_{41}) - |\Omega_c|^2]$  ( $\Delta\omega_D = k_s v_T$  is Doppler width), which can be rewritten as

$$K(\omega) = \frac{\omega}{c} + \tilde{\kappa}_{23} \frac{\sqrt{\pi}(\omega + i\gamma_{41})}{(\omega - \omega_+)(\omega - \omega_-)}, \quad (\text{D2})$$

with  $\omega_{\pm} = -i(\gamma_{21} + \gamma_{41} + \Delta\omega_D)/2 \pm \sqrt{[|\Omega_c|^2 - |\Omega_{\text{ref}}|^2]}$  and  $\Omega_{\text{ref}} = |\gamma_{21} + \Delta\omega_D - \gamma_{41}|/2$ . Equation (D2) is similar to Eq. (15), with difference only in  $\omega_{\pm}$  and  $\Omega_{\text{ref}}$  which are now dependent on  $\Delta\omega_D$  due to the Doppler effect.

From Eq. (D2) one can obtain the gain spectrum  $-\text{Im}(K)$ , which can be decomposed in different control-field regions by using the SDM. Similar formulas (like (16)-(18)) and



figure (like Fig. 5) can be obtained, which are omitted here. From these results we can acquire the following conclusions: (i) In the weak control field region,  $-\text{Im}(K)$  is the sum of two Lorentzian terms centered at  $\omega = 0$ , which have opposite signs. The superposition of the two Lorentzian terms results in a quantum destructive interference and hence a gain doublet appears in the gain spectrum. (ii) In the strong control field region,  $-\text{Im}(K)$  can be approximately expressed as a sum of two Lorentzian terms, which however have the same sign, locate at different positions, and far apart each other. Thus in this region the gain spectrum is an ATS one because there is no interference occurring. (iii) In the intermediate control field region, which is the region between the weak and the strong ones, the gain spectrum displays a crossover from the quantum destructive interference to the ATS.

In a similar way, one can make similar calculations for the GAN and GAL-II systems. The general conclusions obtained in Sec. III and Sec. IV are not changed when Doppler effect is taken into consideration. However, QI characters in the GAN and GAL-II systems with Doppler effect display differences in comparison with that without Doppler effect, some of which have been described in Fig. 7.

- 
- [1] P. W. Milonni, *Fast Light, Slow Light and Left-handed Light* (Inst. Phys. Pub., Bristol, 2005).
  - [2] K. B. Khurgin and R. S. Tucker (ed), *Slow Light: Science and Applications* (Boca Raton, Taylor and Francis, 2009).
  - [3] M. Fleischhauer, A. Imamoglu, and J. P. Marangos, “Electromagnetically induced transparency: Optics in coherent media,” *Rev. Mod. Phys.* **77**, 633 (2005).
  - [4] L. Deng, M. G. Payne, “Gain-assisted large and rapidly responding Kerr effect using a room-temperature active Raman gain medium,” *Phys. Rev. Lett.* **98**, 253902 (2007).
  - [5] Slow light (fast light) refers to the situation in which the group velocity of a light pulse  $V_g \ll c$  ( $V_g > c$  or negative) [1].
  - [6] R. W. Boyd and D. J. Gauthier, “Slow and Fast Light,” *Progress in Optics* (Elsevier Science, 2002), Vol. 43, Chap. 6, p. 275 and references therein.
  - [7] R. W. Boyd and D. J. Gauthier, “Controlling the velocity of light pulses,” *Science* **326**, 1704 (2009).
  - [8] S. Chu and S. Wong, “Linear pulse propagation in an absorbing medium,” *Phys. Rev. Lett.*

- 48**, 738 (1982).
- [9] R. Y. Chiao, “Superluminal (but causal) propagation of wave packets in transparent media with inverted atomic populations,” *Phys. Rev. A* **48**, R34 (1993).
- [10] A. M. Steinberg and R. Y. Chiao, “Dispersionless, highly superluminal propagation in a medium with a gain doublet,” *Phys. Rev. A* **49**, 2071 (1994).
- [11] L. J. Wang, A. Kuzmich, A. Dogariu, “Gain-assisted superluminal light propagation,” *Nature* **406**, 277 (2000).
- [12] M. S. Bigelow, N. N. Lepeshkin, R. W. Boyd, “Superluminal and slow light propagation in a room-temperature solid,” *Science* **301**, 200 (2003).
- [13] G. S. Agarwal, S. Dasgupta, “Superluminal propagation via coherent manipulation of the Raman gain process,” *Phys. Rev. A* **70**, 023802 (2004).
- [14] K. J. Jiang, L. Deng, and M. G. Payne, “Ultraslow propagation of an optical pulse in a three-state active Raman gain medium,” *Phys. Rev. A* **74**, 041803 (2006).
- [15] K. J. Jiang, L. Deng, and M. G. Payne, “Superluminal propagation of an optical pulse in a Doppler-broadened three-state single-channel active Raman gain medium,” *Phys. Rev. A* **76**, 033819 (2007).
- [16] G. Huang, C. Hang, and L. Deng, “Gain-assisted superluminal optical solitons at very low light intensity,” *Phys. Rev. A* **77**, 011803(R) (2008).
- [17] C. Hang, and G. Huang, “Giant Kerr nonlinearity and weak-light superluminal optical solitons in a four-state atomic system with gain doublet,” *Opt. Express* **18**, 2954 (2010).
- [18] H. Li, L. Dong, C. Hang, and G. Huang, “Gain-assisted high-dimensional self-trapped laser beams at very low light levels,” *Phys. Rev. A* **83**, 023816 (2011).
- [19] C. J. Zhu, C. Hang, and G. Huang, “Gain-assisted giant Kerr nonlinearity in a  $\Lambda$ -type system with two-folded lower levels,” *Eur. Phys. J. D* **56**, 231 (2010).
- [20] C. J. Zhu, and G. Huang, “High-order nonlinear Schrödinger equation and weak-light superluminal solitons in active Raman gain media with two control fields,” *Opt. Express* **19**, 1963 (2011).
- [21] R. B. Li, L. Deng, and E. W. Hagley, “Fast, All-Optical, Zero to  $\pi$  Continuously Controllable Kerr Phase Gate,” *Phys. Rev. Lett.* **110**, 113902 (2013).
- [22] C. Tan and G. Huang, “Surface polaritons in a negative-index metamaterial with active Raman gain,” *Phys. Rev.* **91**, 023803 (2015).

- [23] C. Hang and G. Huang, “Highly entangled photons and rapidly responding polarization qubit phase gates in a room-temperature active Raman gain medium,” *Phys. Rev. A* **82**, 053818 (2010).
- [24] A. Lezama, A. M. Akulshin, A. I. Sidorov, P. Hannaford, “Storage and retrieval of light pulses in atomic media with “slow” and “fast” light,” *Phys. Rev. A* **73**, 033806 (2006).
- [25] J. B. Clark, R. T. Glasser, Q. Glorieux, U. Vogl, T. Li, K. M. Jones, and P. D. Lett, “Quantum mutual information of an entangled state propagating through a fast-light medium,” *Nat. Photon.* **8**, 515 (2014).
- [26] G. S. Agarwal, “Nature of the quantum interference in electromagnetic-field-induced control of absorption,” *Phys. Rev. A* **55**, 2467 (1997).
- [27] T. Y. Abi-Salloum, “Electromagnetically induced transparency and Autler-Townes splitting: two similar but distinct phenomena in two categories of three-level atomic systems,” *Phys. Rev. A* **81**, 053836 (2010).
- [28] P. M. Anisimov, J. P. Dowling, and B. C. Sanders, “Objectively discerning Autler-Townes splitting from electromagnetically induced transparency,” *Phys. Rev. Lett* **107**, 163604 (2011).
- [29] L. Giner, L. Veissier, B. Sparkes, A. S. Sheremet, A. Nicolas, O. S. Mishina, M. Scherman, S. Burks, I. Shomroni, D. V. Kupriyanov, P. K. Lam, E. Giacobino, and J. Laurat, “Experimental investigation of the transition between Autler-Townes splitting and electromagnetically-induced-transparency models,” *Phys. Rev. A* **87**, 013823 (2013).
- [30] C. Tan, C. Zhu, and G. Huang, “Analytical approach on linear and nonlinear pulse propagations in an open  $\Lambda$ -type molecular system with Doppler broadening,” *J. Phys. B* **46**, 025103 (2013).
- [31] C. Zhu, C. Tan, and G. Huang, “Crossover from electromagnetically induced transparency to Autler-Townes splitting in open V-type molecular systems,” *Phys. Rev. A* **87**, 043813 (2013).
- [32] C. Tan and G. Huang, “Crossover from electromagnetically induced transparency to Autler-Townes splitting in open ladder systems with Doppler broadening,” *J. Opt. Soc. Am. B* **31**, 704 (2014).
- [33] Peng. B, S. K. Ozdemir, W. J. Chen, F. Nori, L. Yang, “What is and what is not electromagnetically induced transparency in whispering-gallery microcavities,” *Nat. Commun.* **5**, 5085 (2014).
- [34] J. Ding, B. Arigong, H. Ren, M. Zhou, J. Shao, M. Lu, Y. Chai, Y. Lin, and H. Zhang,

- “Tuneable complementary metamaterial structures based on graphene for single and multiple transparency windows,” *Sci. Rep.* **4**, 6128 (2014).
- [35] X. Lu, X. Miao, J. Bai, L. Pei, M. Wang, Y. Gao, L.-A. Wu, P. Fu, R. Wang, and Z. Zuo, “Transition from Autler-Townes splitting to electromagnetically induced transparency based on the dynamics of decaying dressed states,” *J. Phys. B: At. Mol. Opt. Phys.* **48**, 055003 (2015).
- [36] S. Davuluria, Y. Wang and S. Zhu, “Destructive and constructive interference in the coherently driven three-level systems,” *J. Mod. Opt.* **62**, 1091 (2015).
- [37] R. W. Boyd, *Nonlinear Optics* (3rd edition) (Academic, Elsevier, 2008).
- [38] Through the text, all signal fields in the GAN, GAL-I and GAL-II systems are assumed to be weak so that their nonlinear effect is negligible.
- [39] The frequency and wave number of the signal field are given by  $\omega_s + \omega$  and  $k_s + K(\omega)$ , respectively. Thus  $\omega = 0$  corresponds to the center frequency of the signal field.
- [40] A. S. Zibrov, A. B. Matsko, and M. O. Scully, “Four-Wave Mixing of Optical and Microwave Fields,” *Phys. Rev. Lett.* **89**, 103601 (2002).
- [41] E. Kuznetsova, O. Kocharovskaya, P. Hemmer, and M. O. Scully, “Atomic interference phenomena in solids with a long-lived spin coherence,” *Phys. Rev. A* **66**, 063802 (2002).
- [42] H. Lee, Y. Rostovtsev, C. J. Bednar, and A. Javan, “From laser-induced line narrowing to electromagnetically induced transparency: closed system analysis,” *Appl. Phys. B* **76**, 33 (2003).
- [43] L. Li and G. Huang, “Linear and nonlinear light propagations in a Doppler-broadened medium via electromagnetically induced transparency,” *Phys. Rev. A* **82**, 023809 (2010).
- [44] M. Xiao, Y.-q. Li, S.-z. Jin, and J. Gea-Banacloche, “Measurement of Dispersive Properties of Electromagnetically Induced Transparency in Rubidium Atoms,” *Phys. Rev. Lett.* **74**, 666 (1995).
- [45] A. M. Akulshin and R. J. McLean, “Fast light in atomic media,” *J. Opt.* **12**, 104001 (2010).